MASS LOSS OF DENSITY CURRENTS TRAVELLING OVER POROUS BED

Sara Venuleo*[1], Mário J. Franca[2] and Anton J. Schleiss[1],

presenting author, sara.venuleo@epfl.ch [1]Laboratory of Hydraulic Constructions, École Polytechnique Fédérale de Lausanne, Lausanne, Switzerland

[2]Water Science and Engineering Department, IHE Delft Institute for Water Education & Department of Hydraulic Engineering, Delft University of Technology, Delft, The Netherlands

Introduction

Polluted liquids leaking from their storages over the surrounding gravel beds or oil spilling into aquifers, are examples of gravity currents moving over a porous terrain. Density-driven flows provoked by saline or temperature differences or turbidity currents, travelling over fissured lakes and ocean bottoms, may disrupt deposits of gases or fluids, entraining them and eventually releasing them into the environment.

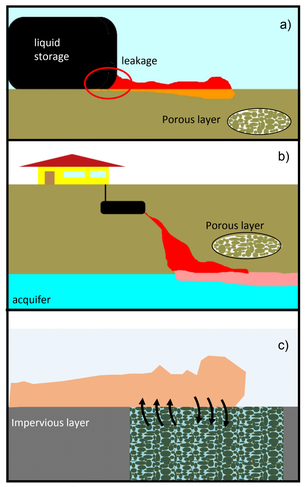

Figure 1: Examples of gravity currents travelling over porous bed: a) Spilling of pollutants, Release of wasted liquids, Incorporation and transport of liquids trapped in natural deposits.

To prevent and confine the environmental impact of such events, it is crucial to understand the mass exchange processes of gravity currents travelling over porous terrains, and how their internal structure is affected by the interaction with the porous bed and by the entrainment of clear water.

Density currents flowing over porous bed have been studied theoretically and experimentally (Lionet and Quoy(1995), Thomas et al.(1998), Moodie and Pascal(1999), Ungarish and Huppert(2000), Marino and Thomas (2002), Thomas et al.(2004), Spannuth et al.(2009), Thomas and Marino(2012)). However, most of these studies deal with lock-exchange experiments and focus on the decrease in front velocity and the distance travelled by the current before extinction.
Conversely, little attention has been given to continuously-fed gravity currents travelling on porous substrates, and the few occurrences of these studies deal with viscous flows.
We here consider inertial (Reb<2000) continuously-fed brine density currents. Given the continuos momentum supply from the inlet, these flows do not estinguish because of their sinking into the bed, as it often observed for lock-exchange currents. On the contrary, after a first phase during which the current sinks into the bottom, the flow starts entraining clear water from the underlying cavities. This entrainment process is not steady in time and its related, for continuity reasons, with the mass loss through the bottom. Both, clear water entrainment and mass loss depend on the momentum of the current, on the porosity of the substrate and on its confinment.
In this study we present how, using the preliminary results of 23 laboratory experiments.

Objectives

In this study we set the following objectives:

- ❑ Quantify the mass loss rate and observe its dependence on the initial excess density and inflow injection velocity.
- ❑ Understand how the boundary condition of the porous substrate affects the sinking (i.e How the current sinking and the clear water entrainment from the bottom are conditioned when the porosity is confined or filled with fluid of the same density of the injected flow).
- ❑ Observe and characterize the dynamics and driving mechanism of the clear-water entrainment from the bottom (i.e. understand if it is driven by shear type instabilities or by Rayleigh-Taylor type instabilities, observe it's evolution in time when the confinement or the porous medium changes).

Experimental program

To fulfill our objectives, we planned 23 experiments reproducing continuously-fed brine gravity currents over beds of different porosity. The set of experiments can be grouped according to inlet inflow-discharge and initial excess density as shown inTable 1. The main bulk parameters of each experiment are also listed, together with the features of the porous substrate on which the current travels. Particularly, the ''non confined'' or ''confined'' feature defines the downstream boundary condition of the porous region: when the porosity is confined this boundary is closed, viceversa, the boundary its open (see Figure 3).
For each experiment we acquired simultaneously density and velocity measurements, as hereafter schematized.

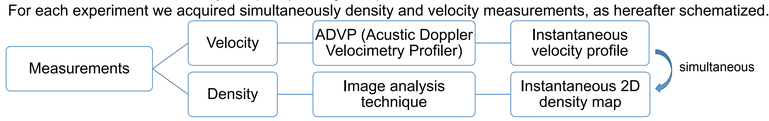

Table1: Main parameters of the performed experiments.

GR BC	name	Inlet Q [l/s]	Initial density [kg/m^3]	Porosity	Prosity BC	Inlet Fr	Inlet Re
A	EXR1006_Q07_P00	0.7	1006	0	-	0.76	2715
	EXR1006_Q07_P12			0.12	non confined		
	EXR1006_Q07_P20			0.2	non confined		
	EXR1006_Q07_P29			0.29	non confined		
	EXR1006_Q07_P42			0.42	non confined		
	EXR1006_Q07_P42F			0.42	Filled		
B	EXR1006_Q14_P00	1.4	1006	0	-	1.44	5431
	EXR1006_Q14_P12			0.12	non confined		
	EXR1006_Q14_P20			0.2	non confined		
	EXR1006_Q14_P29			0.29	non confined		
	EXR1006_Q14_P42			0.42	non confined		
	EXR1006_Q14_P29F			0.29	Filled		
	EXR1006_Q14_P42F			0.42	Filled		
	EXR1006_Q14_P42C			0.42	Confined		
	EXR1006_Q14_P42I			0.42	Ink		
	EXR1006_Q14_P42IF			0.42	Ink-Filled		
C	EXR1020_Q13_P00	1.3	1020	0	-	0.77	4906
	EXR1020_Q13_P12			0.12	non confined		
	EXR1020_Q13_P20			0.2	non confined		
	EXR1020_Q13_P29			0.29	non confined		
	EXR1020_Q13_P42			0.42	non confined		
	EXR1020_Q13_P42F			0.42	Filled		
	EXR1020_Q13_P42C			0.42	Confined		

Experimental methods

- **Experimental facility:**

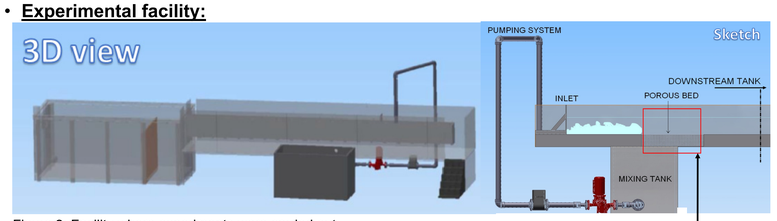

Figure 2: Facility where experiments were carried out.

- **Porosity representation:**

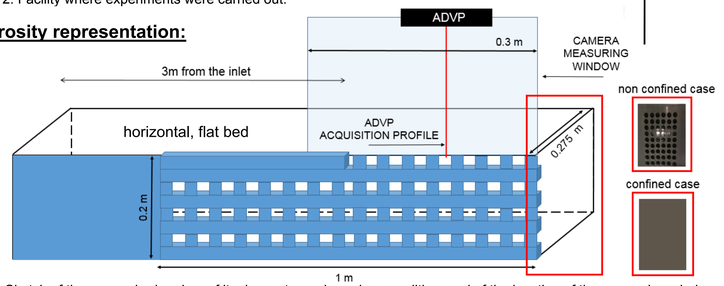

Figure 3: Sketch of the porous bed region, of its down-stream boundary condition, and of the location of the measuring window.

A fissured bed is built in a 1mX 0.2m X 0.275m cavity of the bottom arranging prismatic PVC sticks having quadrangular section of side 2cm. 10 layers of equally spaced sticks are placed alternating a layer of streamwise disposed sticks with a layer of span-wise placed sticks. Different sticks spacing reproduce terrains of varying permeability and porosity.

Table2: Main parameters characterizing bottom cavities.

Porosity	Cavities width w [mm]	Cavities aspect ratio h/w
0.12	2.3	0.115
0.2	5	0.25
0.29	7.5	0.375
0.42	15	0.75

Figure 4: Sketch of the bottom cavities

Figure 5: Layer of the bottom during construction. The two, span-wise and stream-wise PVC sticks layers are here recognizable.

- **Density measurements**: are acquired through an image analysis technique based on ink-light absorption similar to the one applied by Hacker et al. (1996), and Nogueira et al. (2013). The brine water is opportunely inked before injection. The steps of the applied image analysis technique are summarized in Figure 6.

- Backlighting LED panel
- Controlled light conditions
- Basler acA2040-90uc Camera
- Brine water is opportunely inked

Figure 6: Steps of the applied image analysis technique: on the left, the blue color component of the row acquired image, which is transformed into ink concentration map (shown in the center) applying a calibration curve previously obtained with a pixel by pixel calibration. Finally the density distribution (shown on the right), is computed assuming that ink and salt concentration equally dilute. On the right the camera used to acquire the images.

- **Velocity measurements**: an Acoustic Doppler Velocimetry Profiler allows to acquire 3D quasi-instantaneous velocity profiles over the bottom. Its recording frequency is synchronized with the camera shooting at 31.25 Hz.

Figure 8: ADVP sketch, after Blanckaert & Lemmin (2006)
Figure 7: From the top to the bottom: Longitudinal (u) and vertical (w) velocity and time density evolution together with the depth averaged velocity evolution in time (black iine).

Results and discussion

- **Development of a mixing layer at the lower interface of the current**

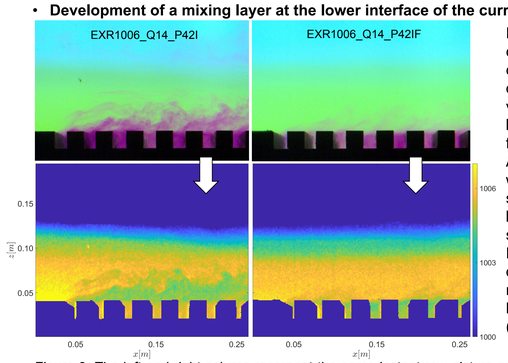

Figure 9: The left and right column represent the same instant raw picture and corresponding density map of two experiments with same inflow condition (B) but respectively when the bed is filled of inked fresh water (left column) and when the bed is filled with inked brine water of the same density of the inlet inflow (right column).

Figure 9 shows two experiments with same inflow condition (B) but respectively when the bed is filled of clear water and when the bed is filled with brine water of the same density of the inlet inflow. To better visualize the formation and evolution of the mixing layer we added permanganate potassium to the water filling the bottom cavities.
Although in both cases some mixing is observed, when the bed is filled of fresh water (experiment shown in the left column), a fully developed mixing layer forms, suggesting that the mass exchange is significantly boosted by Rayleigh-Taylor instabilities. However, as the bed fills with heavier fluid, the density difference at the lower current boundary fades, and mixing gradually starts to be driven by shear, as it happens when the bed is filled with brine water (experiment shown in the right column).

- **Mass loss through the bottom**

To quantify the mass exchange through the lower boundary of the current we considered the mass balance of a reference column, between two sections, upstream (SEC A) and downstream (SEC B) the porosity reach (see Figure 10):

$$M_c(t) = \sum_{t=t\_head}^{t} \left(Q_1(t) - Q_2(t) + Q_I(t) - Q_{bed}(t) \right) dt \quad (1)$$

$$\sum_{t\_t\_head}^{t} Q_{bed}(t) = -M_c(t) + \sum_{t=t\_head}^{t} Q_1(t) - Q_2(t) + Q_I(t) \quad (2)$$

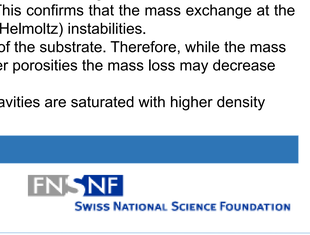

Figure 10: Scheme of the reference flow column, and of the instantaneous fluxes.

The right side of equation (2) is shown in Figure (11) for gr B and gr C experiments. The term QI was found to be negligible. The slope of these curves represents the instantaneous flow discharge through the bottom, and therefore the rate of the mass loss. Note that when the porous substrate is confined, the slope of the curve is initially milder than for curves represnting same porosity unconfined beds. Moreover it, and becomes almost horizontal towards the end of the experiment, indicating the bed saturates with heavier fluid and exchange of mass fades.

Figure 11: Time cumulative sum of the flow entering the bottom, obtained computing the mass balance of the refence column in Figure 10.

Each of the curve of Figure 11 is devided in 3 time windows (t1, t2, t3) having constant slope. This is computed by linear regression to obtain the value of Qbed characterizing that time window. Results of this estimation for the 3 groups of experiments are shown in Figure 12.

Figure 12: Slope of the time cumulative sum of the flow entering the bottom: quantification of the discharge loss rate.

Independently on the inlet conditions, Figure 12 shows that higher porosities and higher inlet velocities correspond to larger mass loss rates. However the discharge sinking into the bottom is not steady in time, and its evolution depend on the void volume of the substrate. For lower porosities the mass loss increase in time, independently on the inflow conditions. However, gr C experiments, over larger porosities, show a mass loss decrease in time, indicating that, the fast sinking due to the high density difference, slows down once the bed is saturated.

Conclusions

Preliminary results show that:

- ❑ Rayleigh-Taylor instabilites boost significantly the mixing in the near bed region. However, as the density difference decreases, they gradually fade until velocity shear becomes the first driver of the mass exchange.
- ❑ The higher the current density and inlet velocity, the larger the mass loss rate. This confirms that the mass exchange at the lower interface is ruled by both static (Rayleigh-Taylor) and shear driven (Kelvin-Helmoltz) instabilities.
- ❑ The higher the porosity and the larger the excess density, the faster is the filling of the substrate. Therefore, while the mass loss of currents travelling over lower porosities is gradually increasing, over larger porosities the mass loss may decrease and fade, due to the drop in the density difference ruling the sinking.
- ❑ Confined porosity substrates fill slower than unconfined substrates. Once their cavities are saturated with higher density fluid, the sinking of the current drops.

Acknowledgements

The presented study is supported by the Swiss National Science Foundation (SNSF Grant Number: 200021 159249).

REFERENCES:

Blanckaert, K., & Lemmin, U. (2006). Means of noise reduction in acoustic turbulence measurements. Journal of Hydraulic Research, 44 , 3–17.
Hacker, J., Linden P. F., and Dalziel S. B. (1996). "Mixing in lock-release gravity currents", Dynamics of Atmospheres and Oceans, 24 (1–4), 183–195.
Lionet, J., and Quoy, O. (1995). ''Gravity currents over porous media.'' Internal Rep., DAMTP, Univ. of Cambridge.
Marino, B. M., and Thomas, L. P. (2002). "The spreading of a gravity current over a permeable surface." J. Hydraul. Eng., 128(5), 527–533.
Moodie, T. B., and Pascal, J. P. (1999). ''Downslope movement of compositionally driven gravity flows over porous surfaces.'' J. Porous Media, 2(2), 127-141
Nogueira H., Adduce C., Alves E., and Franca M., (2013). "Image analysis technique applied to lock-exchange gravity currents," Measurement Science and Technology, 24(4).
Spannuth, M. J., Neufeld, J. A., Wettlaufer, J. S., and Worster, M. G. (2009). "Axisymmetric viscous gravity currents flowing over a porous medium." J. Fluid Mech., 622, 135–144.
Thomas, L. P., Marino, B. M., and Linden, P. F. (1998). ''Gravity currents over porous substrates.'' J. Fluid Mech., 366, 239–258.
Thomas, L. P., Marino, B. M., and Linden, P. F. (2004). "Lock-release inertial gravity currents over a thick porous layer." J. Fluid Mech.,503, 299–319.
Thomas L. P. and Marino B. M. (2012) "Inertial density currents over porous media limited by different lower boundary conditions", *Journal of Hydraulic Engineering,* 138(2): 133–142.
Ungarish, M., and Huppert, H. E. (2000). ''Gravity currents over a porous boundary: shallow-water solutions and box-model approximations.''J. Fluid Mech., 418.